Wideband Vertically Polarized Antenna with Endfire Radiation for 5G Mobile Phone Applications

Faizi Khajeim, Maryam; Moradi, Gholamreza; Shirazi, Reza Sarraf; Zhang, Shuai; Pedersen, Gert Frølund

Published in:
I E E E Antennas and Wireless Propagation Letters

DOI (link to publication from Publisher):
10.1109/LAWP.2020.3009097

Publication date:
2020

Document Version
Accepted author manuscript, peer reviewed version

Wideband Vertically Polarized Antenna with Endfire Radiation for 5G Mobile Phone Applications

Maryam Faizi Khajeim, Gholamreza Moradi, *Senior Member*, *IEEE,* Reza Sarraf Shirazi, Shuai Zhang, *Senior Member*, *IEEE*, and Gert Frølund Pedersen, *Senior Member*, *IEEE*

***Abstract*—This letter presents a wideband slotted substrate integrated waveguide (SIW) antenna for millimeter-wave 5G mobile handset applications. The antenna is vertically polarized and has a small clearance of 3.3 mm. To realize a wide operating bandwidth, two sets of vias are employed to perform a change in SIW height. Furthermore, a pair of U-shaped slots is used in both top and bottom faces of SIW to improve impedance matching and front to back radiation ratio. The antenna achieves a measured –6-dB bandwidth of 35.7 % (23.4-33.6 GHz) and a –10-dB bandwidth of 17.4 % (26.2-31.2 GHz). The beamforming capability of the antenna array is investigated. The antenna array has good scanning performance and achieves large spatial coverage.**

***Index Terms*—Endfire radiation, handset antenna, millimeter-wave, phased array, vertical polarization, wideband.**

I. Introduction

In order to provide higher data rates required by new applications in the future, the fifth-generation (5G) cellular communication systems have been established. The millimeter-wave (mm-wave) is one of the key 5G technologies, where obtaining wider bandwidth is easier than 4G/LTE cellular system. However, there are several important issues that should be considered in mm-wave bands. Increasing the frequency would result in a high free space path loss. Therefore, the gain of antennas in mobile phones and base stations needs to be increased to compensate losses without using more transmitted power. The concept of using phased arrays in 5G has been proposed to solve the problems caused by losses [1]–[5].

According to 3GPP 5G specification (Release 15) [6], four frequency bands between 24250 MHz and 40000 MHz are allocated for 5G new radio. It is important to design a mm-wave antenna covering wideband. In the new generation of mobile phones, the dimension of an LCD screen is increased. A very small space in ungrounded portions of the mobile phone is available to place the mm-wave antennas. So 5G mm-wave handset arrays are required to have small clearance. Several antennas with end-fire [7]–[10] and broadside [11]–[13] radiation patterns have been designed for mm-wave 5G applications. Some investigations considering antenna and user interactions [14], [15] show that employing antennas with endfire radiations would lead to relatively fewer user effects on antenna performance. Furthermore, mm-wave handset antennas with vertical polarization are also needed in practical applications. However, due to the thin substrate in handsets and since the electric field is in the vertical direction, it is very challenging to design vertically polarized mm-wave antennas with broad impedance bandwidth, good radiation performance, and small thickness, simultaneously, while wideband horizontally polarized microstrip antennas could be thin.

In this letter, we propose a compact wideband antenna with small clearance, vertical polarization and endfire radiation patterns for 5G mobile handset applications. Two sets of vias and a pair of slots are used to produce two resonances, which enable the antenna to achieve wide operating bandwidth. Moreover, two slots act as magnetic currents and radiate simultaneously with the open end of the SIW and improve front to back radiation ratio of the antenna [16], [17]. The performance of the designed antenna is investigated with CST Microwave Studio (CST MWS) software and verified experimentally.

This letter is organized as follows: The structure and analysis of the proposed single element antenna are presented in section II. Section III investigates the antenna array performance, while Section IV compares simulated and measured results. Finally, a conclusion is given in section V.

II. Single Element Analysis and Design

The structure of the single radiating element is shown in Fig. 1. The antenna is printed in a three-layer stack-up PCB with two prepreg layers between them. The material of three layers is Rogers RO4003C (ε_r = 3.38, tanδ = 0.0025) with a

Manuscript received March 31, 2020; revised June 9, 2020; accepted July 7, 2020. Date of publication November 1, 2020; date of current version April 16, 2019. This work was supported in part by the Iran National Science Foundation, and in part by the AAU Young Talent Program. (Corresponding author: Gholamreza Moradi).

M. Faizi Khajeim, G. Moradi and R. Sarraf Shirazi are with the Microwave Measurement Research Laboratory, Department of Electrical Engineering, Amirkabir University of Technology (Tehran Polytechnic), Iran, Tehran 15875 4413 (e-mail: mfaizi@aut.ac.ir; ghmoradi@aut.ac.ir; sarraf@aut.ac.ir).

S. Zhang and G. F. Pedersen are with the Department of Electronic Systems, Aalborg University, 9220 Aalborg, Denmark (e-mail: sz@es.aau.dk; gfp@es.aau.dk).

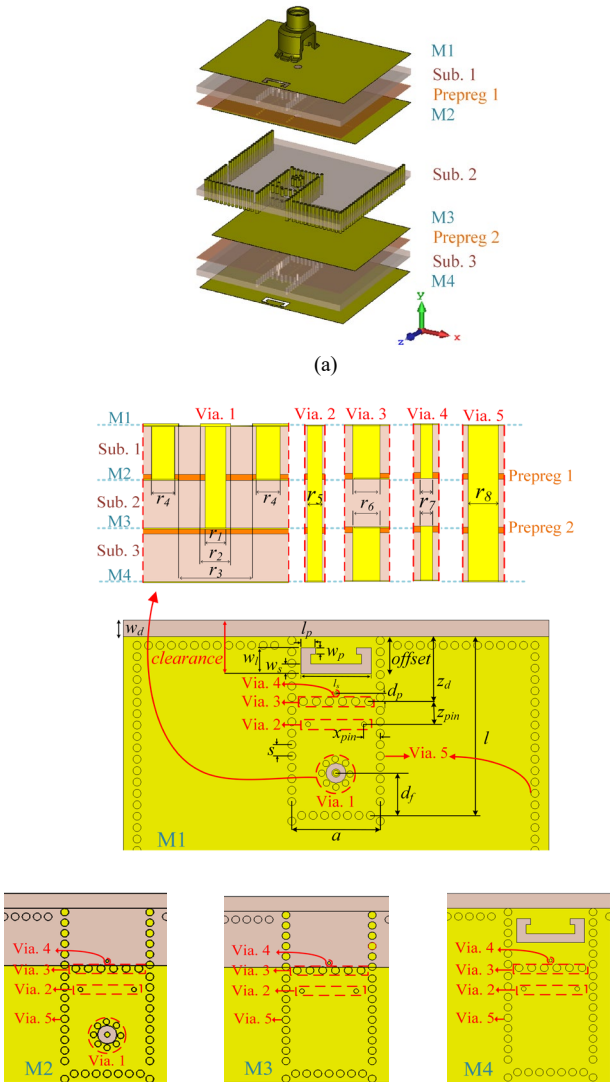

Fig. 1. Antenna configuration. (a) Exploded view. (b) Dimensions and layers.

thickness of 0.813 mm and the prepreg is Rogers RO4450F (ε_r = 3.7, tanδ = 0.004) with a thickness of 0.1 mm. The thickness of all copper layers is 18 μm. As illustrated in Fig. 1(b), by inserting a set of vias symmetrically in Sub. 1 and Sub. 3 (see Via 3 in Fig. 1 (b)), a change in the thickness of the SIW is obtained. This discontinuity is in E field direction of the TE_{10} mode inside the SIW and places a shunt capacitance across the SIW, which is dependent on SIW thickness variation [18]. Therefore, the element can reach the required impedance matching. Furthermore, a pair of U-shaped slots is employed in both top and bottom broad faces of SIW, which produce another resonance for the radiating element. Therefore, by realizing two resonances, a wide operating bandwidth could be achieved. Part of the substrate is extended to perform a loading for the aperture, which tunes the real part of input impedance [19].

Fig. 2(b) shows the electric field distribution on the slots and open end. According to the equivalence principle, two magnetic currents on the top and bottom slots could be defined

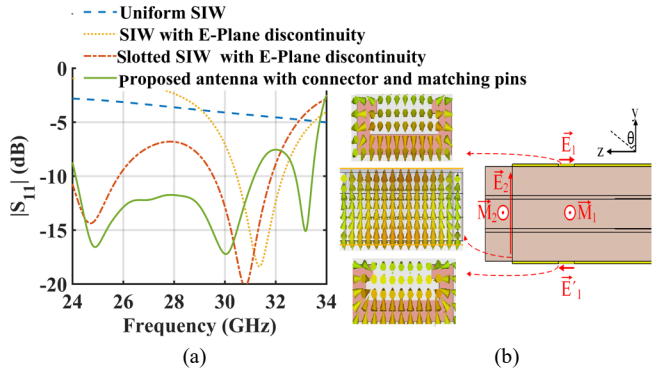

Fig. 2. (a) The reflection coefficient of the proposed single element and comparison with other configurations. (b) Equivalent magnetic currents of the electric field on the slots and open end of the SIW at 29 GHz.

using $-n \times \vec{E}$. Two magnetic currents radiate together and result in a semi omnidirectional pattern. Therefore, two magnetic currents on the slots can be regarded as an equivalent magnetic current M_1 at the position of the slots. Moreover, the open end of the SIW has a semi omnidirectional pattern as well. Using the equivalence principle, the open end can be regarded as a magnetic current M_2 in the x direction. The total radiated field by the M_1 and M_2, is equal to the sum of the two and in the y-z plane is given by:

$$\vec{E}(\theta,\phi) = \vec{e}_1(\theta,\phi) + e^{jk_0 \sin\theta\,(\text{offset}-w_s/2)}\vec{e}_2(\theta,\phi) \qquad (1)$$

$\vec{e}_1(\theta,\phi)$ and $\vec{e}_2(\theta,\phi)$ are the element pattern of M_1 and M_2, respectively.

If M_1 and M_2 have the same magnitude and proper phase difference, the resultant radiation pattern would be unidirectional. The waves radiated by M_1 and M_2 would be in phase toward positive z direction (θ = 90˚), and would be out of phase toward negative z direction (θ = –90˚). The magnitude of M_1 is dependent on the length and width of the slots, while the phase difference between M_1 and M_2 is dependent on the distance of slots from the open end.

Increasing the length and width of the slots, would increase the magnitude of M_1, making it closer to the magnitude of M_2. In order to achieve the proper dimension of the slots, both the reflection coefficient and the radiation pattern, should be considered simultaneously.

The simulated S_{11} of the single element is shown in Fig. 2(a). As illustrated, the return loss of a uniform SIW without any change in height, is less than 5 dB. In the SIW with the E-plane discontinuity, a resonance at 31.3 GHz is achieved. Another resonance appears at 24.6 GHz, when two U-shaped slots are etched in the broad faces of the SIW. Increasing the width of the slot increases the frequency of the first mode, while increasing the length of the slot decreases the frequency of the first mode and the frequency of the second mode does not change significantly.

The proposed single radiating element achieves wide operating bandwidth of 24.7 % (24.1-30.9 GHz), which covers n257, n258 and n261 in 3GPP 5G specification. Fig. 1(a) shows a single element antenna integrated with an MMPX connector. Layers M1 to M4 show copper layers in the

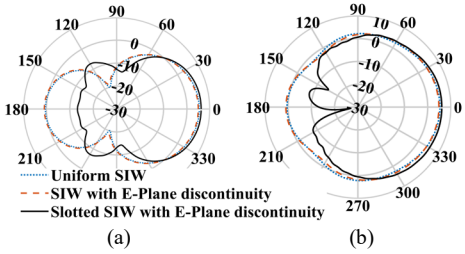

Fig. 3. The radiation pattern of the proposed antenna and comparison with other configurations at the center frequency in the (a) H–Plane. (b) E–Plane.

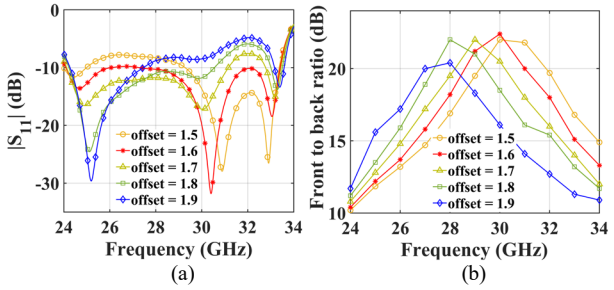

Fig. 4. The impact of the slots distance from the open end on the (a) reflection coefficient and (b) front to back radiation ratio.

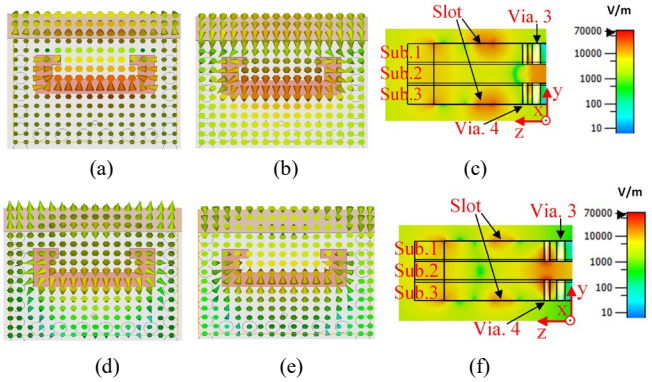

Fig. 5. The electric field distribution at the first mode on the (a) top face, (b) bottom face, (c) vertical cross section and at the second mode on the (d) top face, (e) bottom face, (f) vertical cross section.

antenna structure. Two grounding pins (see Via. 2 in Fig. 1 (b)) are employed in the feeding SIW transmission line to provide a proper transition from a coaxial transmission line to SIW. Also, a pair of pins (see Via. 4 in Fig. 1 (b)) is inserted at the center of the SIW in Sub. 1 and Sub. 3, which acts as a capacitive loading and improves antenna impedance matching.

In order to extend feeding coaxial line up to Sub. 2, a set of vias in a circular design is inserted in Sub. 1 (see Via.1 in Fig. 1 (b)). The optimized design parameters were: a = 5.4, l = 11, *offset* = 2.3, w_d = 1, w_s = 0.6 , l_s = 4, w_l = 1.6, l_p = 0.6, w_p = 0.4, z_d = 4, d_p = 0.5, x_{pin} = 1, z_{pin} = 1.4, s = 0.7, d_f = 2.6, r_1 = 0.34, r_2 = 0.5, r_3 = 1.23, r_4 = 0.4, r_5 = 0.3, r_6 = 0.5, r_7 = 0.2, r_8 = 0.5 (all in millimeters).

The simulated radiation patterns of the proposed single element and comparison with other configurations at the center frequency are shown in Fig. 3. As illustrated, adding the slots improves the front to back radiation ratio significantly.

The impact of the distance of the slots from the open end on the S_{11} and the front to back radiation ratio is demonstrated in Fig. 4(a) and (b), respectively. Increasing the offset, improves the impedance matching in the first mode, while degrades it in the second mode. As demonstrated, at offset = 1.7 mm, a good impedance matching for both modes and wide operating bandwidth is achieved. Increasing the offset improves front to back radiation ratio in lower frequencies. The distance between slots and open end determines the phase difference between two magnetic currents. Therefore, when distance increases, the frequency in which phase difference meets the required condition to suppress the back lobe, decreases.

Fig. 5 shows the simulated E-field distributions for two operating modes of the antenna. As illustrated, the electric field is dominant on the slots in the first mode, while in the second mode, it is dominant around Via. 3 and Via. 4. This confirms the concept of operation discussed previously.

III. Antenna Array

According to the link budget and 3GPP requirements in millimeter-wave bands [20], a quad-element antenna array is capable to provide the required gain in mobile handsets. The simulated reflection coefficients of the port 1 and 2 of the array and the radiation patterns at the center frequency are shown in Fig. 6(a) and (b), respectively. As illustrated, both ports have good impedance matching over the operating frequency band.

The antenna array is designed on a 70.2 mm wide ground plane and the inter-element spacing is 5.4 mm. All four MMPX connectors are mounted on the M1 layer.

In order to investigate antenna array scanning performance, ports are excited with equal magnitude and progressive phase shift. Fig. 7 demonstrates antenna array scanning performance at the center frequency. As illustrated, considering the threshold gain of 7 dBi, the antenna array is capable to cover –46° to +46°, where the gain is above threshold gain.

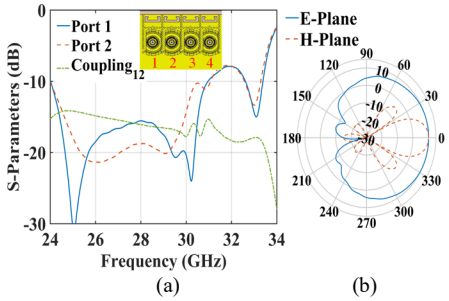

Fig. 6. (a) The reflection coefficient of the antenna array for port 1 and port 2. (b) The radiation pattern of the antenna array.

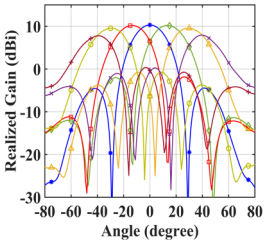

Fig. 7. The scanning performance of the antenna array at the center frequency of the operating band.

TABLE I
COMPARISON BETWEEN DIFFERENT MM-WAVE ANTENNAS POTENTIAL FOR MOBILE PHONE APPLICATIONS

References	Operating Band (GHz)	Beam Direction	Thickness	Clearance	4×1 Array Gain (dBi)	Array $HPBW_{Elevation}$	Scan Range
[7]	26.3-29.75	End-fire	0.07 λ_0	0.46 λ_0	9.98	114	N.A
[8]	50-77.8	End-fire	0.47 λ_0	0.53 λ_0	N.A	110	± 51°
[9]	27-29	End-fire	0.46 λ_0	0.65 λ_0	12.61	133.1	N.A
[11]	26.5-29.7	Broadside	0.2 λ_0	0.46 λ_0	13.9	79.6	N.A
[12]	56.6-64.2	Broadside	0.3 λ_0	1 λ_0	13.2	N.A	± 42°
This work	$26.2\text{-}31.2_{Measured}$ $24.2\text{-}31_{Simulated}$	End-fire	0.24 λ_0	0.3 λ_0	10.3	136	± 46°

IV. EXPERIMENTAL RESULTS

Fig. 8 shows the fabricated antenna array and measurement setup. The measurement was performed in the anechoic chamber at Aalborg University. The measured S-Parameters are illustrated in Fig. 9. Since all four ports have similar performances, the simulated and measured results of port 2 are illustrated. Due to the fabrication imperfection, in the measured reflection coefficients, one of the modes shifts to other frequencies. Therefore, the measured reflection coefficient is slightly worse than the simulated, but it is still better than -7 dB, which is sufficient for mobile handset antennas. The simulated and measured radiation patterns at different frequencies within the operating band are shown in Fig. 10. The simulated and measured radiation patterns align very well and the radiation patterns are stable within the whole operating band.

(a) (b)

Fig. 8. (a) The fabricated antenna array. (b) The radiation pattern measurement setup.

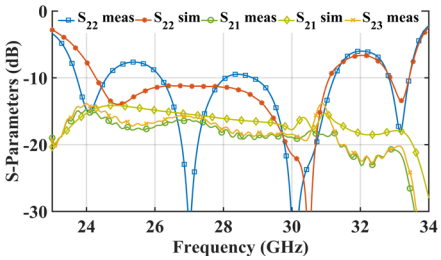

Fig. 9. The simulated and measured S–Parameters of the proposed antenna.

A comparison between the proposed antenna and the previous works is presented in Table I. In this work, in comparison with the previously reported antennas, clearance is considerably decreased, while wide frequency bandwidth with good radiation performance and small thickness is obtained.

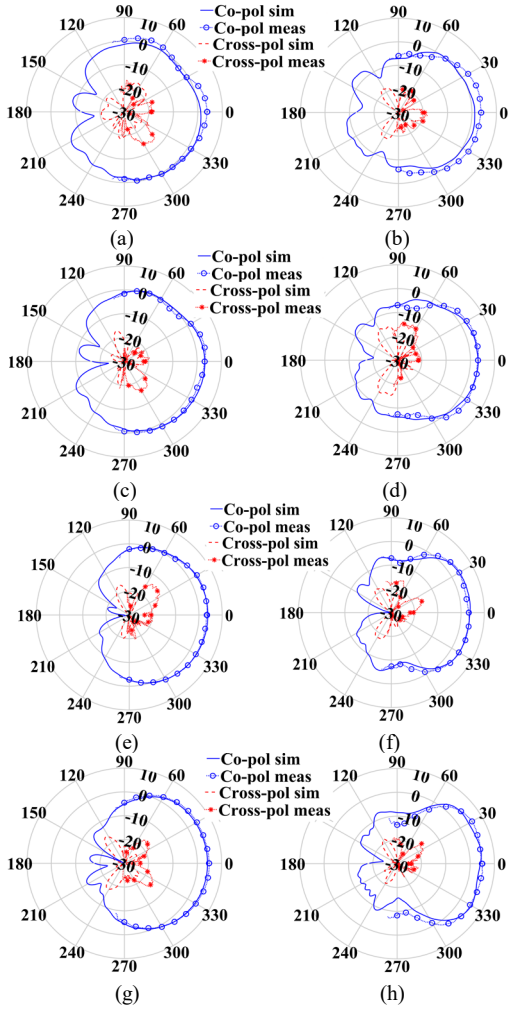

Fig. 10. The simulated and measured radiation patterns of element 2 in the array at 24 GHz in the (a) E–Plane and (b) H–Plane. At 26 GHz in the (c) E–Plane and (d) H–Plane. At 28 GHz in the (e) E–Plane and (f) H–Plane. At 30 GHz in the (g) E–Plane and (h) H–Plane.

V. CONCLUSION

A wideband antenna array for 5G handset has been proposed. Two sets of vias and two U-shaped slots in top and bottom faces were used to increase the operating frequency bandwidth and the front to back ratio. The good radiation performance, wide frequency bandwidth and compact configuration make the proposed antenna an appropriate candidate to be integrated in the 5G mobile phone devices.

REFERENCES

[1] J. G. Andrews, S. Buzzi, W. Choi, S. V. Hanly, A. Lozano, A. C. Soong, and J. C. Zhang, "What will 5G be?" *IEEE Journal on selected areas in communications*, vol. 32, no. 6, pp. 1065-1082, Jun 2014.

[2] I. A. Hemadeh, K. Satyanarayana, M. El-Hajjar, and L. Hanzo, "Millimeter-wave communications: Physical channel models, design considerations, antenna constructions, and link-budget," *IEEE Communications Surveys & Tutorials*, vol. 20, no. 2, pp. 870-913, Dec 2017.

[3] S. Zhang, X. Chen, I. Syrytsin, and G.F. Pedersen, "A Planar switchable 3-D-coverage phased array antenna and its user effects for 28-GHz mobile terminal applications," *IEEE Transactions on Antennas and Propagation*, vol. 65, no. 12, pp. 6413-6421, Dec 2017.

[4] N. Ojaroudiparchin, M. Shen, S. Zhang, and G.F. Pedersen, "A switchable 3-D-coverage-phased array antenna package for 5G mobile terminals," *IEEE Antennas and Wireless Propagation Letters*, vol. 15, pp. 1747-1750, Feb 2016.

[5] W. Hong, K. H. Baek, and S. Ko, "Millimeter-wave 5G antennas for smartphones: Overview and experimental demonstration," *IEEE Transactions on Antennas and Propagation*, vol. 65, no. 12, pp. 6250-6261, Dec 2017.

[6] TS38.101-2 v15.0.0 User Equipment (UE) radio transmission and reception; Part 2: Range 2 Standalone (Release 15), Jun 2018.

[7] I. J. Hwang, B. Ahn, S. C. Chae, J. W. Yu, and W. W. Lee, "Quasi-yagi antenna array with modified folded dipole driver for mmWave 5G cellular devices," *IEEE Antennas and Wireless Propagation Letters*, vol. 18, no. 5, pp. 971-975, Mar 2019.

[8] Y. Li, and K. M. Luk, "A multibeam end-fire magnetoelectric dipole antenna array for millimeter-wave applications," *IEEE Transactions on Antennas and Propagation*, vol. 64, no. 7, pp. 2894-2904, April 2016.

[9] W. El-Halwagy, R. Mirzavand, J. Melzer, M. Hossain, and P. Mousavi, "Investigation of wideband substrate-integrated vertically-polarized electric dipole antenna and arrays for mm-wave 5G mobile devices," *IEEE Access*, vol. 6, pp. 2145-2157, Dec 2017.

[10] J. Wang, Y. Li, L. Ge, J. Wang, and K. M. Luk, "A 60 GHz horizontally polarized magnetoelectric dipole antenna array with 2-D multibeam endfire radiation," *IEEE Transactions on Antennas and Propagation*, vol. 65, no. 11, pp. 5837-5845, Sep 2017.

[11] S. J. Park, D. H. Shin, and S. O. Park, "Low side-lobe substrate-integrated-waveguide antenna array using broadband unequal feeding network for millimeter-wave handset device," *IEEE Transactions on Antennas and Propagation*, vol. 64, no. 3, pp. 923-932, Dec 2015.

[12] J. Zhu, B. Peng, and S. Li, "Cavity-backed high-gain switch beam antenna array for 60-GHz applications," *IET Microwaves, Antennas & Propagation*, vol. 11, no. 12, pp. 1776-1781, Jul 2017.

[13] T. Deckmyn, M. Cauwe, D. V. Ginste, H. Rogier, and S. Agneessens, "Dual-Band (28, 38) GHz Coupled Quarter-Mode Substrate-Integrated Waveguide Antenna Array for Next-Generation Wireless Systems," *IEEE Transactions on Antennas and Propagation*, vol. 67, no. 4, pp. 2405-2412, Jan 2019.

[14] V. Raghavan, M. L. Chi, M. A. Tassoudji, O. H. Koymen, and J. Li, "Antenna placement and performance tradeoffs with hand blockage in millimeter wave systems," *IEEE Transactions on Communications*, vol. 67, no. 4, pp. 3082-3096, Jan 2019.

[15] A. R. Guraliuc, M. Zhadobov, R. Sauleau, L. Marnat, and L. Dussopt, "Near-field user exposure in forthcoming 5G scenarios in the 60 GHz band," *IEEE Transactions on Antennas and Propagation*, vol. 65, no. 12, pp. 6606-6615, Nov 2017.

[16] M. F. Khajeim, G. Moradi, R. S. Shirazi, P. Mousavi, M. Sohrabi, K. Jamshidi, and D. Plettemeier, "A Compact End-Fire Slotted SIW Antenna Array for 5G Mobile Handset," In *IEEE 2nd 5GWF,* Dresden, Germany, 2019, pp. 126-129.

[17] Y. Luo, and J. Bornemann, "Substrate integrated waveguide horn antenna on thin substrate with back-lobe suppression and its application to arrays," *IEEE Antennas and Wireless Propagation Letters*, vol. 16, pp. 2622-2625, Aug 2017.

[18] D.M. Pozar, "Microwave network analysis," in *Microwave engineering*, 4th ed., John Wiley & Sons, 2009, pp. 203-209.

[19] H. Wang, D. G. Fang, B. Zhang, and W. Q. Che, "Dielectric loaded substrate integrated waveguide (SIW) H-Plane horn antennas," *IEEE Transactions on Antennas and Propagation*, vol. 58, no. 3, pp. 640-647, Mar 2010.

[20] Y. S. Yeh, B. Walker, E. Balboni, and B. Floyd, "A 28-GHz phased-array receiver front end with dual-vector distributed beamforming," *IEEE Journal of Solid-State Circuits*, vol. 52, no. 5, pp. 1230-1244, Dec 2016.